

## A GREEN APPROACH FOR THE SYNTHESIS OF DRUG DELIVERY SYSTEM, MESOPOROUS SILICA GRAFTED ACRYLAMIDE - $\beta$ - CYCLODEXTRIN COMPOSITE, FOR THE CONTROLLED RELEASE OF CURCUMIN

MANOHAR D MULLASSERY\*, NOELINE B FERNANDEZ, SURYA R, DIANA THOMAS

Department of Chemistry, Fatima Mata National College, Kollam - 691 001, Kerala, India. Email: mdmullassery@gmail.com

Received: 18 April 2018, Revised and Accepted: 02 June 2018

### ABSTRACT

**Objective:** The scope of the present study was the preparation and characterization of a novel composite acrylamide  $\beta$ -cyclodextrin grafted 3-aminopropyltriethoxysilane bentonite (AMCD-g-APSB), for the controlled delivery of curcumin (CUR).

**Methods:** AMCD-g-APSB, was synthesized by solvent-free conditions using microwave irradiation. The structure and surface morphology of the composite was established using Fourier transform infrared spectroscopy, X-ray diffraction, scanning electron microscopy, thermal analysis, etc.

**Results:** The swelling percentage of the composite depends on both time and pH of the medium. The maximum swelling of the composite occurred at a pH of 7.4. The maximum drug encapsulation was occurring at a pH 3. About 96.5% of drug was loaded at pH 3. *In vitro* biocompatibility study was performed, and the result showed good biocompatibility of the composite in the concentration range 2.5–50  $\mu$ g/ml.

**Conclusions:** Drug delivery study of the composite proved that CUR could be successfully released in a controlled manner in the colon without much losses of the drug in the stomach.

**Keywords:** Bentonite, Controlled release, Curcumin, Kinetics.

© 2018 The Authors. Published by Innovare Academic Sciences Pvt Ltd. This is an open access article under the CC BY license (<http://creativecommons.org/licenses/by/4.0/>) DOI: <http://dx.doi.org/10.22159/ajpcr.2018.v11i9.26769>

### INTRODUCTION

Cancer is a group of disease involving abnormal cell growth with the potential to spread to other parts of the body. Over 100 types of cancer affect human. According to WHO, cancer is the second leading cause of death globally. Chemotherapy is one of the major treatments of cancer. However, chemotherapy has many limitations such as uncontrolled drug toxicity, undesirable side effects, etc. Researchers over the last two decades concentrated on the investigation studies of anticancerous drugs with comparatively low side effects. Curcumin (CUR) is identified as one of the natural compounds with significant efficiency and less toxic. CUR is a bioactive component of the food additive *Curcuma Longa* which is widely used in Asian countries. The number of cancer patients in south Asian countries are relatively low, this may due to the more consumption of turmeric as dietaries [1,2].

The bright yellow-orange color of turmeric is due to the fat-soluble polyphenolic pigments known as curcuminoids. CUR is the principal curcuminoid found in turmeric. The chemical formulae and molecular weight of CUR are  $C_{21}H_{20}O_6$  and 368.38 g/mol respectively. IUPAC name is (1E, 6E)-1,7-bis(4-hydroxy-3-methoxyphenyl)-1,6-heptadiene-3,5-dione. CUR has two aromatic ring systems containing o-methoxy phenolic groups, linked with a seven carbon linker consisting of an  $\alpha$ ,  $\beta$ -unsaturated and  $\beta$ -diketone moiety, as shown in Fig. 1. CUR undergoes keto-enol tautomerism, in nonpolar and moderately polar solvent, enol form of CUR is more stable to exist than the ketoform [2]. Preclinical and clinical studies show that CUR exerts anti-inflammatory, anti-oxidant, anticancerous, neuroprotective, and antidiabetic activities. Many studies were reported on the anticancerous activity of CUR against colon, liver, pancreatic, ovarian, and breast cancers [3,4].

CUR has some important drawbacks such as its low water solubility, rapid hydrolysis under high alkaline conditions, and susceptibility to photochemical degradation. It also exhibits poor absorption, rapid

metabolism, and low bioavailability. These limitations can be overcome by the use of a biocompatible and novel drug carrier system for the effective encapsulation and successive release of CUR to the targeted site without losing its anticancerous activity [5].

The mesoporous silica materials can be used as a potential drug carrier system for the controlled and targeted drug delivery. Hence, many studies have been reported in porous silica-based materials as drug carriers [6-8]. Table 1 shows different kinds of modified mesoporous systems used as drug delivery systems. Mesoporous materials have tunable pore size; it can change its pore size from 2 to 50 nm. Hence, this material can be used as a better drug carrier system for different kinds of bioactive materials of with variable size [9].

Montmorillonite belongs to the smectite group, composed of silica tetrahedral sheets layered between alumina octahedral sheets at the ratio of 2:1, respectively. The mineral composition of bentonite is quite variable depending on its origin. In general, sodium montmorillonite represents the main components in these clays (up to 80% by weight). However, for the development of bentonite-based controlled release formulations, their properties must be needed to modify for improving their affinity for bioactive drug molecules. Intercalation of polymer matrix onto clay scaffold is one of the treatment techniques is gaining attention, as the composite hydrogel has got the combined advantages of biodegradability of polymer matrix and tunable pore size of the mesoporous silica.

In the present study, a biocompatible pH-sensitive composite was prepared by the grafted copolymerization of  $\beta$ -cyclodextrin - acrylamide (AMCD) intercalated by the modified 3-Aminopropyltriethoxysilane bentonite (APSB) for the controlled release of CUR [16]. During the intercalation, a calculated amount of ethylene glycol dimethacrylate (EGDMA) was used a crosslinker agent because it can form stable networks by withstanding wide range of pH and temperature [17].

Table 1: List of different kinds of modified mesoporous silica materials as drug delivery system

Drug delivery system	Drug	Reference
Montmorillonite-poly lactic-coglycidic acid composite	Insulin	[10]
Amino functionalized mesoporous nanomaterial	5-Flurouracil	[11]
Alginate encapsulated mesoporous silica	Indomethacin	[12]
Amine functionalized cubic mesoporous silica material	CUR	[13]
3-aminopropyltriethoxysilane modified mesoporous silica material	CUR	[14]
Chitosan mesoporous silica material	CUR	[2]
Carboxymethyl cellulose grafted mesoporous silica material	CUR	[15]
Present study	CUR	

CUR: Curcumin

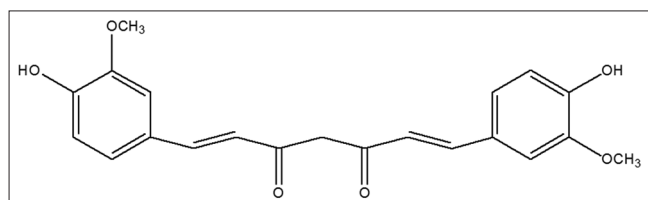


Fig. 1: Structure of curcumin

The intercalated composite of the natural clay (bentonite) with the polysaccharides could retain its properties such as biodegradability, non-toxicity, swelling, behavior, etc. [18]. The grafted composite of clays with the hydrogel can act as a potential drug delivery system [19,20].

## MATERIALS AND METHODS

### Materials

The bentonite clay was procured from Ashapura Clay Mines (Gujarat, India).  $\beta$ -cyclodextrin (CD), EGDMA, CUR were purchased from Tokyo Chemical Industry (Japan). AM was received from Merck Life Science Pvt. Ltd (India). Ceric ammonium nitrate (CAN) was obtained from Merck Specialities Pvt. Ltd (India). Acetone and  $\alpha$ ,  $\alpha$ -azobisisobutyronitrile (AIBN) and 3-aminopropyl triethoxysilane were procured from Spectrochem Pvt., Ltd (India). Dulbecco's Modified Eagle's Medium (DMEM), 3-(4, 5-dimethylthiazol-2-yl)-2, and 5-diphenyltetrazolium bromide (MTT) were purchased from Himedia (Mumbai, India). U87MG glioma cell line was provided by NCCS (Pune, India). The pH of the medium was adjusted using phosphate and citrate buffer. Distilled water with specific conductivity  $<1 \mu\text{S}/\text{cm}$  was used throughout the study. The stock solution of CUR was prepared in ethanol. CUR solution was freshly prepared for each and every day use.

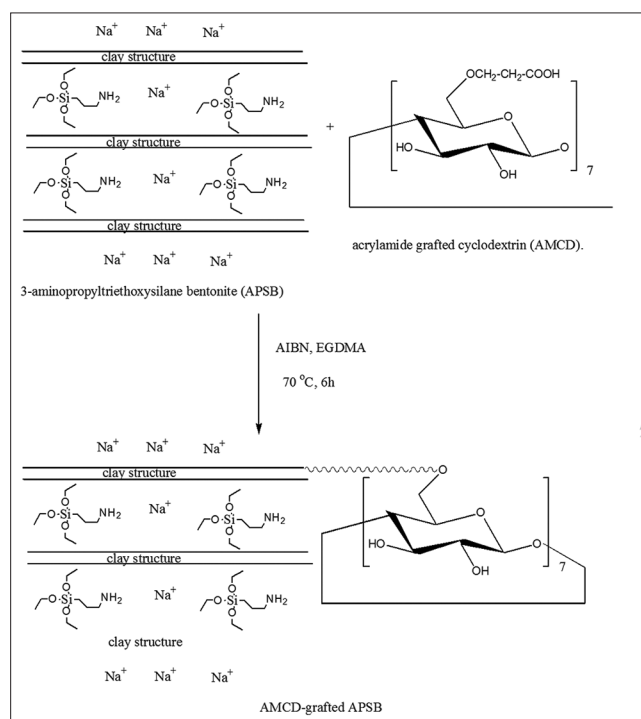
### Synthesis of the drug delivery system (AMCD-g-APSB) involves the following steps

#### Preparation of APSB

About 10 g of powdered bentonite was dispersed in excess of 1 M NaCl solution and kept for 24 h. The solution was centrifuged and washed with distilled water till it was completely free from chloride ions. After the removal of chloride ions, the clay was dried at  $80^\circ\text{C}$  and grained to powder. About 5.0 g of Na-B was dried at  $60^\circ\text{C}$  for 24 h and dispersed in 100 ml of methanol. Separately, a solution with 5 g of 3-aminopropyltriethoxysilane (pur) was dissolved in 100 ml solvent. This solution was added to the dispersion containing Na-Bentonite [21]. The dispersion was stirred at  $50^\circ\text{C}$  under magnetic stirring for 72 h. After complete stirring, the product was centrifuged and washed with distilled water, dried at  $80^\circ\text{C}$  and grained to fine powder.

#### Solvent-free synthesis of AMCD

The grafted copolymer derived from AAm (pure) and  $\beta$ -CD (pure) was prepared by microwave assisted, free radical-induced polymerization method. About, 1.0 g  $\beta$ -CD was dispersed in 120 ml of water and 5 g of AM was mixed with 30 ml of water and added to  $\beta$ -CD-water mixture and stirred for 1 h. 300 mg of CAN (pure) was dissolved in 30 ml of water and added to the above dispersion [22-25]. The dispersion was



Scheme 1: Preparation of acrylamide  $\beta$ -cyclodextrin grafted 3-aminopropyltriethoxysilane bentonite

irradiated by microwave for 2 min. It was left for overnight and then precipitated using acetone (pure). The unreacted monomer and other reagents were removed by washing with aqueous ethanol (30%, v/v). The grafted polymer was then dried at  $40^\circ\text{C}$  to a constant weight and converted to fines.

#### Preparation of AMCD-grafted-APSB

The preparation of AMCD-g-APSB was represented in Scheme 1. About 5.0 g of APSB, 2.5 g of AMCD, 0.50 g of EGDMA and 0.04 g of AIBN were added to a three neck RB flask which was equipped with a magnetic stirrer and a reflux condenser. To the above mixture, 25 ml of methanol was added, and the flask was purged by dry  $\text{O}_2$  free  $\text{N}_2$  for 30 min. The mixture was heated at  $70^\circ\text{C}$  for 5 h and stirred continuously (1250 rpm). The product obtained was separated by filtration and washed well with distilled water and methanol (30%, v/v) to remove the by-products. The product was dried at  $60^\circ\text{C}$  and kept overnight and ground to an average particle size of 0.095 mm.

### Characterization

The Fourier transform infrared spectroscopy (FTIR) spectral analysis was performed in transmission mode using a Bruker spectrophotometer (Germany). Spectral scanning was done at  $4 \text{ cm}^{-1}$  resolutions with 32 scans over spectral range from 400 and  $400 \text{ cm}^{-1}$ . XRD studies were used to find out the crystallinity of a substance. X-ray diffraction (XRD) measurements were carried out on a Rigaku Geigerflex XRD meter with

Ni filtered Cu K $\alpha$  radiation at 40 kV, 20 mA. The thermal analyses were made on a Mettler Toledo Star system under nitrogen atmosphere with a heating rate of 20°C min<sup>-1</sup>. A Philips model XL 30 CP scanning electron microscope (SEM) was used to take micrographs. In this instrument, cryofreezing method was used for taking SEM photographs at 15 kV and 20 kV with a working distance of 6 mm, in which freeze samples were coated with a thin layer of gold to make the surface conductive toward electron beam. The pH of the medium was measured using a pH meter (Systronic model  $\mu$  362, India). Absorbance of CUR in the drug carrier was conducted by UV-Visible spectrophotometer (Systronics, India) at  $\lambda_{max}$  of 428 nm.

#### Swelling studies

Swelling of drug carrier systems was important in the effective and targeted delivery of drugs. The swelling behavior of the sample was studied as a function of pH (2 to 9). The pH of the solution was adjusted by varying concentrations of NaOH and HCl. The samples were immersed in excess aqueous medium of desired pH for 10 h to achieve the equilibrium. The swollen samples were then separated and excess surface adhered water molecules were removed by blotting. It was then dried in an air oven at 50°C until there was no change in the dried mass of the sample. The percentage equilibrium water uptake can be calculated as (Equation 1).

$$\text{Swelling (\%)} = \frac{W_{wet} - W_{dry}}{W_{dry}} \times 100 \quad (1)$$

#### Stability study of CUR at different pH conditions

The stability study of CUR was carried out at different pH conditions of 2, 4, 6, 7, and 8. A stock solution of CUR was prepared by dissolving about 5 mg of CUR in 100 ml of methanol-distilled water mixture (60:40 v/v). Each experiment was carried out in dark conditions, incubated at 37  $\pm$  1°C in citrate buffer and phosphate buffer. At definite time intervals, 5 ml of the solution was pipetted out, filtered, and measured for the concentration using the UV-visible spectrophotometer (Systronics, India) at  $\lambda_{max}$  of 428 nm.

#### Drug encapsulation efficiency studies

About 0.1 g of the composite and CUR solution at an initial concentration of 50 mg/l were taken in amber-colored stoppered bottle and stirred at 1000 rpm for 6 h. To get the maximum encapsulation, the analysis was carried out at different pH range of 2–7. The encapsulation study was also repeated for another CUR concentration of 75 mg/l. Along with the encapsulation efficiency study of CUR onto the drug delivery composite AMCD-g-APSB, a comparative study was also done with APSB, a precursor unit of the composite. The percentage of drug encapsulation efficiency was calculated as (Equation 2).

$$\text{DEE} = \frac{\text{Total Curcumin} - \text{Free Curcumin}}{\text{Total Curcumin}} \times 100\% \quad (2)$$

#### In vitro drug release study

Release study of CUR from AMCD-g-APSB and APSB were investigated on different pH conditions of 2.4  $\pm$  0.2, 6  $\pm$  0.2, and 7.4  $\pm$  0.2. About 0.1 g of CUR-loaded AMCD-g-APSB was put in different pH of 2.4, 6, and pH 7.4 separately placed on the water bath shaker of constant temperature of 37  $\pm$  1°C rotated at 100 rpm. At the specified intervals, about 5 ml of the solution was pipetted out and filtered. The concentration of drug release was measured spectrophotometrically. The release studies were performed thrice and the mean percentage was taken as  $\pm$  standard deviation (SD). The cumulative release profile of CUR was calculated and plotted as the percentage of cumulative release against time (Equation 3).

$$\% \text{ of cumulative release} = \frac{\text{Curcumin released}}{\text{Total amount of curcumin loaded}} \times 100 \quad (3)$$

The *in vitro* release kinetics studies were analyzed using the Peppas kinetic relation (Equation 4).

$$\frac{M_t}{M_\infty} = K t^n \quad (4)$$

where  $M_t$  is the amount of drug released at time  $t$  and is the amount of the drug release completely.  $k$  is the rate constant and  $n$  is the diffusion exponential.

#### Cell viability analysis and cell culture conditions

U87MG glioma cells were used as an *in vitro* model for toxicological studies. The U87MG cells were cultured in DMEM under the temperature of 37°C and supplemented with 10% FBS in an atmosphere of 5% CO<sub>2</sub> and a humid atmosphere was maintained. The cells were trypsinized with buffered saline solution containing 0.25% of trypsin and 0.03% of EDTA. The cells were placed to a culture plate for 24 h. MTT assay is a colorimetric assay used for the determination of cell proliferation and cytotoxicity, based on the reduction of the yellow-colored water-soluble tetrazolium dye MTT to formazan crystals. Mitochondrial lactate dehydrogenase produced by live cells reduces MTT to insoluble formazan crystals, which on dissolution into an appropriate solvent exhibits purple color, the intensity of which is proportional to the number of viable cells and can be measured spectrophotometrically at 570 nm. Briefly, seeded using a 200  $\mu$ l cell suspension in a 96-well plate at a cell density of 20,000 cells per well without the test agent. Allow the cells to grow for about 12 h. Add appropriate concentrations of the test agent (2.5  $\mu$ g/ml, 5  $\mu$ g/ml, 10  $\mu$ g/ml, 20  $\mu$ g/ml, and 40  $\mu$ g/ml). Incubate the plate for 24 h at 37°C in a 5% CO<sub>2</sub> atmosphere. After the incubation period, plates are taken from the incubator, and spent media is removed and MTT reagent is added to a final concentration of 0.5 mg/ml of total volume. Wrap the plate with aluminum foil to avoid exposure to light. Return the plates to the incubator and incubate for 3 h. The MTT reagent is removed and then add 100  $\mu$ l of solubilization solution (DMSO). The absorbance is measured on a spectrophotometer at 570 nm and 630 nm is used as a reference wavelength. The cell viability percentage and percentage of cytotoxicity can be calculated by the following equations

$$\text{Cell viability \%} = \frac{\text{Optical density of test}}{\text{Optical density of control}} \times 100 \quad (5)$$

$$\text{Cytotoxicity \%} = 100 - \text{cell viability \%} \quad (6)$$

#### Statistical analysis

All the results were expressed as mean  $\pm$  SD. Statistical analysis was performed with origin 8.0 (Origin -Lab Corporation, USA).

## RESULTS AND DISCUSSION

#### Synthesis of the composite and characterization

Sodium bentonite (NB) was the starting material used in the synthesis of the drug delivery system AMCD-g-APSB. AMCD-g-APSB was formed by the grafting copolymerization of the biocompatible monomer units AMCD and APSB. The grafting synthesis was carried out in the presence of the cross-linking agent EGDMA and the free radical initiator AIBN. The surface of NB was modified by exchanging water molecules with APS in ethanol medium [26]. The water molecules present in the ethanol medium catalyzed the surface silylation of Na-B by APS. Because of the intercalation of the APS, the basal spacing of APSB was increased [27]. The copolymer hydrogel, AMCD can act as a "gate keeper" molecule in which it can be introduced to the tuning pore size of the clay for the effective loading and the controlled release of drug [28-30]. During the synthesis of AMCD from  $\beta$ -CD and AAM, CAN was used as the free radical initiator.

The FTIR spectra of NB, APSB, AMCD, AMCD-g-APSB, CUR, and CUR-L-AMCD-g-APSB were shown in Fig. 2. A broad absorption band observed

at  $3615\text{ cm}^{-1}$  of Na-B represents stretching vibrations of different -OH groups present in Mg-OH-Al, Al-OH-Al and Fe-OH-Al. A strong peak at  $1048\text{ cm}^{-1}$  showed the O-Si-O bending vibration. The peaks at  $545\text{ cm}^{-1}$  and  $460\text{ cm}^{-1}$  represent the bending vibrations of Al-O-Si and Si-O-Si respectively. Another peak at  $950\text{ cm}^{-1}$  corresponds to Al-O-Al bending vibration. The H-O-H bending vibration of water molecules intercalated in the clay mineral was represented by a peak at around  $1628\text{ cm}^{-1}$ . In APSB, two bands were observed nearly at  $1552$  and  $1493\text{ cm}^{-1}$  which can be explained due to the bending vibrations of N-H and  $\text{CH}_2$  group, respectively. Another band at  $3010\text{ cm}^{-1}$  due to the C-N stretching and the bands at  $2860$ - $2924\text{ cm}^{-1}$  represent the C-H vibrations of amino propyl group. The presence of two bands due to -NH and -CH in the spectrum could be considered as an evidence for the intercalation of silane molecules in the clay mineral. After silylation, it can be seen that silane group is present both as covalently bonded to the clay mineral and by hydrogen bonding interaction with intercalated water molecules as evident from the broad band observed in the spectrum of APSB between  $3010$ - $2700\text{ cm}^{-1}$ .

In the FTIR spectrum of AMCD, a characteristic band of ether linkage was found at  $1030$ - $1032\text{ cm}^{-1}$ . The band at  $1628\text{ cm}^{-1}$  may be due to the O-H bending vibrations. Two prominent bands of Am at  $1651$  and  $1602\text{ cm}^{-1}$  were due to the presence of C-O stretching and N-H bending vibrations of amide group, respectively. An overlap band of N-H and O-H stretching peak were observed at  $3188$ - $3499\text{ cm}^{-1}$ . A shoulder at around  $1450\text{ cm}^{-1}$  (C-N str) and a prominent peak at  $1022\text{ cm}^{-1}$  were observed which resulted from the CH-O-  $\text{CH}_2$  group which occurred during grafting reaction.

In the FTIR of AMCD-g-APSB, a peak of -CH-O- $\text{CH}_2$  was shifted to lower intensity. A new peak at  $1205\text{ cm}^{-1}$  observed can be attributed to the C-O-O- stretching vibrations of ester linkage formed between COOH group in the AMCD and the hydroxyl groups of APSB. In the FTIR spectrum of CUR a broad absorption band at  $3520\text{ cm}^{-1}$  was due to phenolic OH group. The aromatic ring of CUR gave two peaks at  $1504$  and  $1435\text{ cm}^{-1}$  resulted from CH bending and CH stretching vibrations,

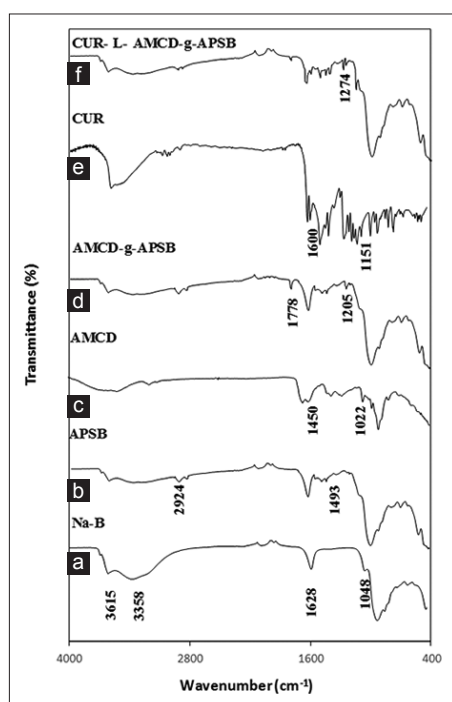


Fig. 2: Fourier transform infrared spectroscopy of (a) Sodium bentonite (b) 3-aminopropyltriethoxysilane bentonite (APSB) (c) acrylamide  $\beta$ -cyclodextrin (AMCD) (d) AMCD-grafted-APSB (AMCD-g-APSB) (e) curcumin (CUR) and (f) CUR-L-AMCD-g-APSB

respectively. Most of the peaks in CUR were retained after loading with DDS showing the effective encapsulation of drug onto composite by weak physical adsorption.

Fig. 3 represents the XRD patterns of NB, APSB, AMCD, AMCD-g-APSB, Cur-L-AMCD and g-APSB. NB showed a peak at  $2\theta = 6.89$  of basal spacing  $13.02\text{ \AA}$ . After silylation, the basal spacing was increased to  $d_{001} = 21.15\text{ \AA}$  which resulted in the lowering of  $2\theta$  value to  $4.17$ . In APSB, a new peak was appeared [19] which correspond to  $d_{002}$  reflection. Compared to the XRD spectrum of NB the increase in basal spacing of APSB by  $8.13\text{ \AA}$  is an evidence for the successive intercalation of 3-aminopropyltriethoxysilane moiety. The broad peaks in the XRD of AMCD indicate the amorphous behavior of the polymer formed. Successful grafting led to an increase in amorphous nature and the swelling features. In the XRD of AMCD-g-APSB, the peaks of APSB were retained and a broad peak indicated the successful grafting of AMCD on APSB. The XRD pattern of the composite and the drug-loaded composite had no remarkable changes as evident from the Figure.

The TG and DTG curves of NB, APSB, AMCD, AMCD-g-APSB, and CUR-L-AMCD-g-APSB were shown in Fig. 4. For NB dehydration at temperature below  $100^\circ\text{C}$  was initially observed, which may be due to the elimination of weakly adsorbed water molecules on the edges and in the interlayer space. Similar behavior was also shown by APSB which showed weight loss up to  $100^\circ\text{C}$ . The weight loss of APSB was higher than that of NB possibly due to the presence of intercalated silane molecules. Three distinct mass loss events were observed in the DTG curve of APSB between  $240^\circ\text{C}$  and  $640^\circ\text{C}$ . These correspond to the loss of silane molecules that were weakly adsorbed by hydrogen bonding, intercalated and chemically bonded to the clay mineral, respectively. The observed initial mass loss at around  $80^\circ\text{C}$  for AMCD was explained for the presence of moisture, solvents, and unreacted monomers. However, no mass loss occurred at the later stage up to  $250^\circ\text{C}$ . The weight loss at  $275^\circ\text{C}$ ,  $375^\circ\text{C}$ , and  $575^\circ\text{C}$  correspond to breaking of rigid polymer network. Compared to AMCD, the composite AMCD-g-APSB was thermally more stable and showed no weight loss after  $430^\circ\text{C}$ .

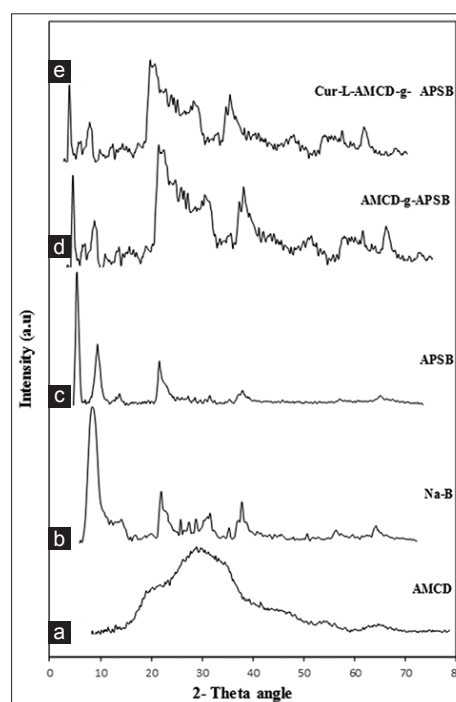
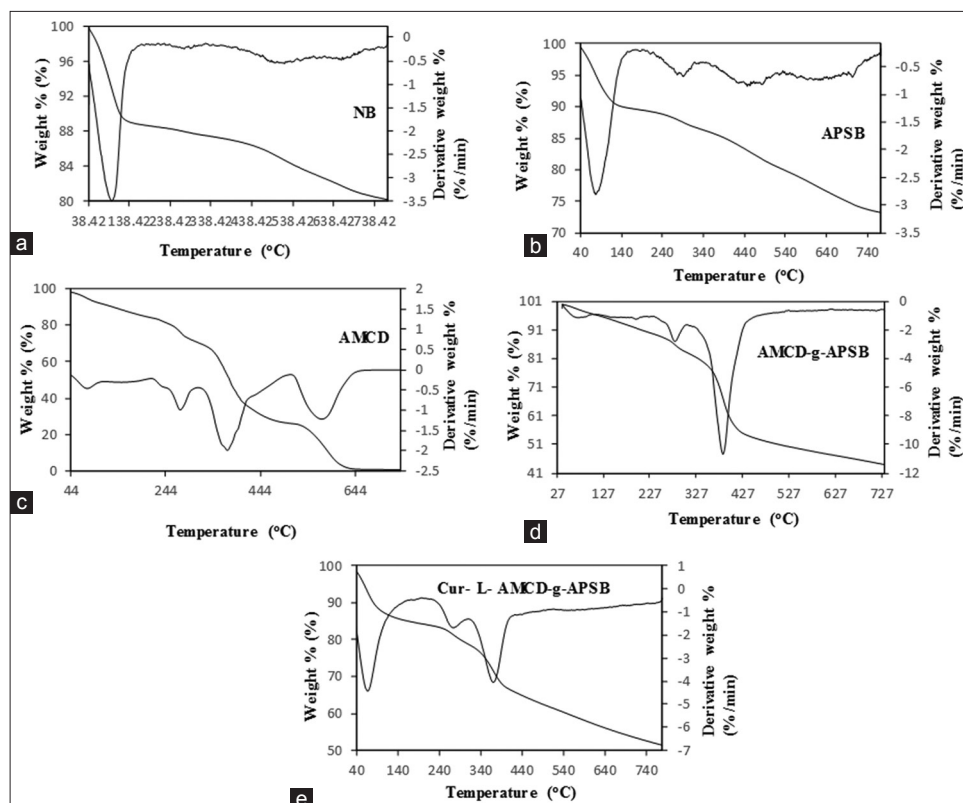


Fig. 3: X-ray diffraction of (a) acrylamide  $\beta$ -cyclodextrin (AMCD) (b) sodium bentonite (c) 3-aminopropyltriethoxysilane bentonite (APSB) (d) AMCD-grafted-APSB (AMCD-g-APSB) (e) curcumin-L-AMCD-g-APSB



**Fig. 4:** Thermogravimetry-differential thermal analysis of (a) Sodium bentonite (b) 3-aminopropyltriethoxysilane bentonite (APSB) (c) acrylamide  $\beta$ -cyclodextrin (AMCD) (d) AMCD-grafted-APSB (AMCD-g-APSB), and (e) curcumin-L-AMCD-g-APSB

It showed four distinct weight loss events. The initial loss in weight below 100°C may be due to the loss of moisture from the composite. According to the literature, the weight loss observed for AMCD-g-APSB between 300 and 400°C can be attributed to the loss of intercalated APS molecules in the interlayer of NB. The TG and DTG curves of drug loaded composite showed three mass loss events. The initial weight loss was due to loss of moisture followed by two mass loss events which was due to the rupture of CUR moiety which was loaded onto DDS.

The SEM images of APSB, AMCD, AMCD-g-APSB, and CUR-loaded AMCD-g-APSB were shown in Fig. 5. The NB has corn flake-like crystals with fluffy appearance revealing its extremely fine platy structure (figure not shown). Compared with the morphology of NB, the image of APSB appeared as individual clubbed particle. The surface of AMCD appeared rough with porous nature. These regular pores were connected to each other to form capillary channels. In general, the inorganic particles with polar lamellae and the hydrophobic units (3-aminopropyl triethoxy part in the silylating agent) undergo aggregation [17]. The surface of AMCD-g-APSB appeared to be irregular due to the presence of larger number of pore cavities. The surface of CUR-loaded AMCD-g-APSB seen to be as regular and homogeneous, due to the loading of CUR in the pore cavities.

The swelling profile of the composite at different pH and at different time intervals were shown in Fig. 6. The swelling percentage of the composite strongly depends on both time and pH of the medium. For acidic pH, the swelling percentage was lower than that in alkaline pH condition. The minimum swelling index was at pH 2, and maximum was at pH 7.4. The swelling of the composite increases with pH and attains a maximum at pH 7.4 and then gradually decreases. In high-pH medium (7.4), the hydrophilic groups(-OH) on the composite were getting ionised and the electrostatic repulsion between these negative charges led to the high swelling of the composite; however, in acidic medium, the absence of swelling caused the collapse of AMCD-g-APSB. Similar results were reported by Anirudhan and Sandeep [31].

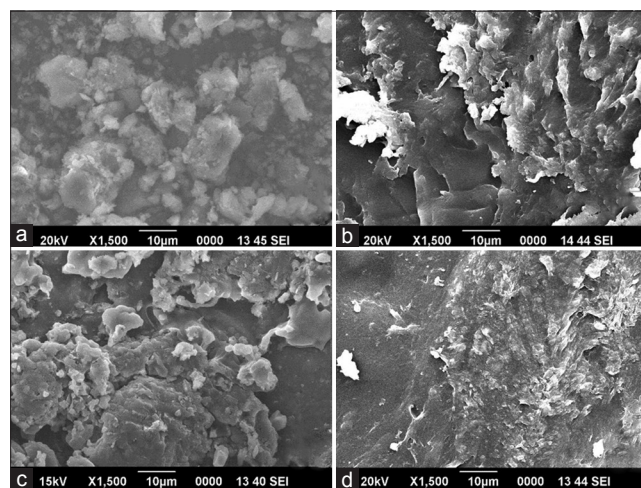


**Fig. 5:** Scanning electron microscope images of (a) grafted 3-aminopropyltriethoxysilane bentonite (APSB) (b) acrylamide  $\beta$ -cyclodextrin (AMCD) (c) AMCD-grafted-APSB (AMCD-g-APSB) and (d) curcumin-L-AMCD-g-APSB

The swelling process was found to be very fast and reached a maximum at 60 min after that it was slowly increased. The initial burst in swelling of the composite may be due to the presence of the hydrophilic group on the surface of AMCD-g-APSB. After 60 min, the decrease in rate of swelling can be attributed to the entering of water molecules in the internal boundary of the clay molecules which is initially not exposed to water molecules. Similar swelling pH dependencies were reported in the case of other composite hydrogels [32].

The physical and the chemical stability of CUR deeply depend on the pH [33] and light [21]. CUR undergoes photochemical degradation;

therefore, all studies are carried out in amber-colored bottle. CUR was unstable at alkaline pH conditions. About 90% of CUR was degraded at the pH of 7.4 with in initial 15 min. At the same time, the stability of CUR at acidic pH was very high, only 3.4% of the drug was degraded within 6 h. The half-life period of CUR on the pH 3, 5, 6, 7, and 8 are 118.63, 199.08, 195.69, 9.40, 1.05 and 14.04 min respectively. The high stability of CUR at acidic conditions may due to the presence of conjugated diene moiety. On increasing the pH (alkaline conditions), the -OH group at phenol gets easily deprotonated which causes the degradation [34]. The result of the present analysis on the stability study of CUR was compared with previous results and was found to be in good agreement [35].

The various formulation parameters in the synthesis of the composite were given in Table 2. The percentage of encapsulation was increased with increase in amount of AMCD. After attaining an optimum value of 2.5 g, the encapsulation efficiency and the swelling percentage is decreased. This can be explained by the fact that with increasing the amount of AMCD, the diffusion of the drug molecules into the internal pore cavities of the clay gets decreased. The encapsulation efficiency also depends on the cross-linking agent. The optimum amount of cross-linking agent is found to be 0.5 g. On increasing the amount of cross linker over the optimum value of 0.5 g, the encapsulation capacity of the composite is getting decreased. This may due to compound formation of EGDMA itself with the composite and the composite becomes more rigid and the pore volume gets decreased [36].

The encapsulation study of CUR onto the composite AMCD-g-APSB was carried out at different pH conditions from 2 to 7. For comparison, the drug encapsulation study of the monomer unit of the composite (APSB) was also carried out. In the case of composite, the drug encapsulation was occurring maximum (96.5%) at a pH of 3. Whereas, the encapsulation of drug onto APSB at the same pH of 3 was only 81%. The encapsulation study of AMCD-g-APSB and APSB at different pH conditions were represented in Fig. 7. In the case of APSB, there was a weak interaction between the -NH<sub>2</sub> group present in the functionalized bentonite and the phenolic -OH group present in the CUR. With increase in the -NH<sub>2</sub> functionalization on the clay surface, the encapsulation efficiency increases. The higher efficiency of AMCD-g-APSB compared to APSB is due to the weak interaction of CUR molecules with cone such as cavities of  $\beta$ -CD apart from interlayer cavities of clay. Moreover, the AMCD is behaving as a gate keeper which may regulate the entering and release of the drug molecules in the composite. The encapsulation efficiency of the composite depends on the amount of the monomers, cross-linking agent and also the pH of the medium. Acrylamido-2-methylpropane sulfonic acid grafted N-maleoylchitosan intercalated montmorillonite showed encapsulation efficiency of 94% [31] whereas alginate/chitosan-coated mesoporous silica-based nanocarriers showed a value of 85.7% [36]. The AMCD-g-APSB (present study) showed higher encapsulation efficiency of 96.1% compared with other mesoporous silica materials. Therefore, it can be concluded that the prepared composite hydrogel is effective for the controlled and targeted delivery of therapeutics.

### In-vitro release analysis

The controlled release study was carried out at different pH of 2.4, 6, and 7.4 at the body temperature condition of 37°C was shown in Fig. 8. The maximum release of drug was seen at pH 6. About 78.5% of drug was released within 48 h at pH 6.0. About 20% of the drug was released slowly within initial 10 h. After that, there was a controlled release of the drug. At the pH of 2.4, release of drug was comparably less, about 25.6% of drug was released within 48 h. Similarly, the release percentage (38.1%) of drug at pH 7.4 was also relatively small. The release of drug is related with the swelling index of the polymer. The maximum swelling of the polymer among three different pH are 7.4>6>2.4. However, the release of drug is in the following order of 6>7.4>2.4. This may due to the fact that the CUR is unstable at pH 7.4.

The release study was also done for the monomer unit APSB, under the same procedure as carried out for AMCD-g-APSB. For APSB, the drug release was maximum at the pH 6 (41.2%) and also shows a minimum

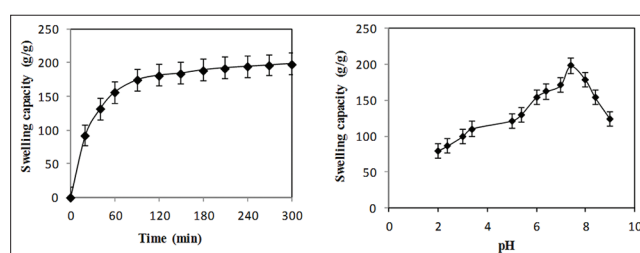


Fig. 6: Swelling study of the composite acrylamide  $\beta$ -cyclodextrin-grafted 3-aminopropyltriethoxysilane bentonite at different time intervals and at different pH (triplicates for each sample were analyzed and each datum point represents the mean value $\pm$ standard deviation; n=3)

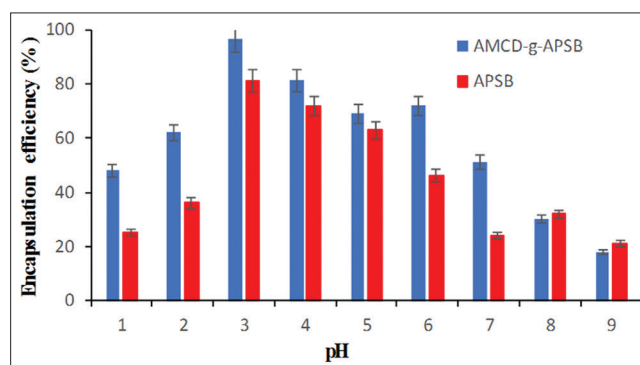


Fig. 7: Percentage of encapsulation efficiency of the acrylamide  $\beta$ -cyclodextrin-grafted 3-aminopropyltriethoxysilane bentonite (APSB) and APSB as a function of pH (triplicates for each sample were analyzed and each datum point represents the mean value $\pm$ standard deviation; n=3)

Table 2: Formulation parameters used in the synthesis of AMCD-g-APSB composite

Sample code	APSB/g	AMCD/g	Cross linking agent/g	Swelling % of the composite (g/g)	Encapsulation efficiency (%)
A1	5	0.5	0.5	92 $\pm$ 1.0	49 $\pm$ 0.28
A2	5	1.0	0.5	109 $\pm$ 0.5	52 $\pm$ 0.86
A3	5	1.5	0.5	124 $\pm$ 1.5	60 $\pm$ 0.57
A4	5	2.0	0.5	131 $\pm$ 1.3	63 $\pm$ 0.28
A5	5	2.5	0.5	200 $\pm$ 1.3	96.1 $\pm$ 2.0
A6	5	5.0	0.5	86 $\pm$ 0.57	45 $\pm$ 2.1
A7	5	2.5	1.0	99 $\pm$ 1.0	50.5 $\pm$ 1.7
A8	5	2.5	0.75	119 $\pm$ 0.76	56 $\pm$ 3.0
A9	5	2.5	0.5	200 $\pm$ 1.3	96.1 $\pm$ 2.0
A10	5	2.5	0.25	162 $\pm$ 1.9	81 $\pm$ 2.0

All the results are expressed as $\pm$ SD. SD: Standard deviation, AMCD-g-APSB:  $\beta$ -cyclodextrin grafted 3-aminopropyltriethoxysilane bentonite

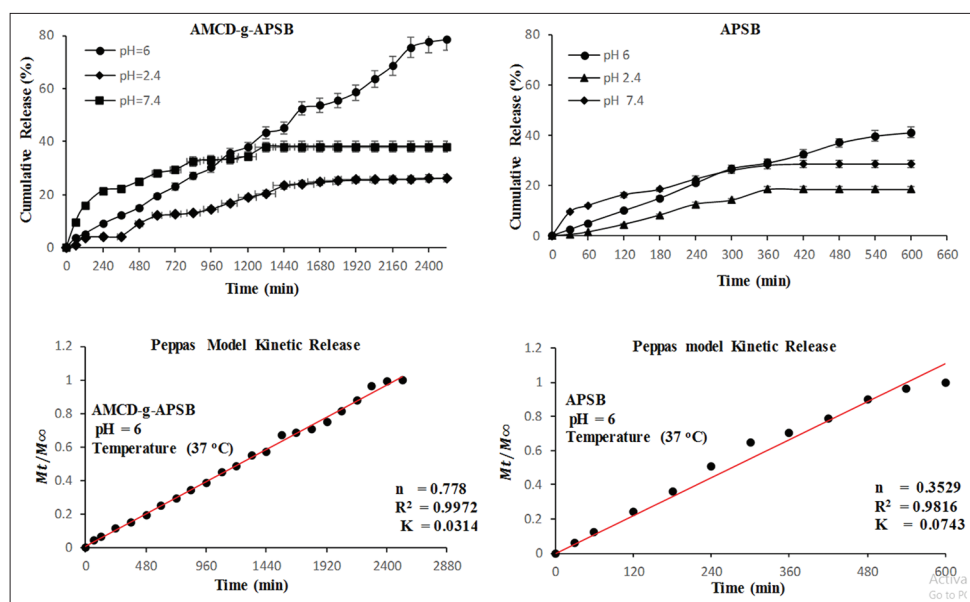


Fig. 8: *In vitro* release of curcumin from AMCD-grafted 3-aminopropyltriethoxysilane bentonite (AMCD-g-APSB) and APSB and the corresponding Peppas kinetic model (triplicates for each sample were analyzed and each datum point represents the mean value $\pm$ standard deviation; n=3)

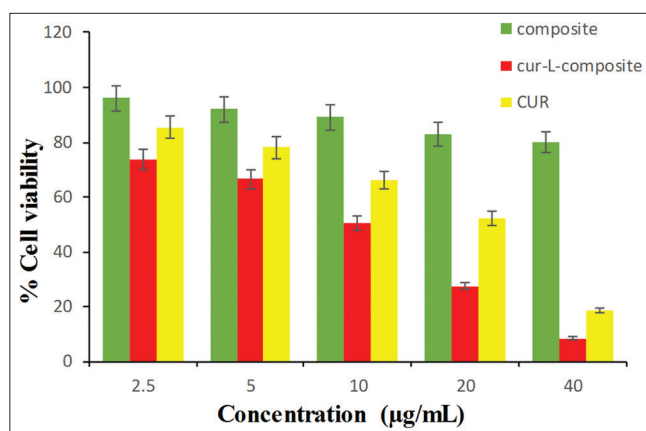


Fig. 9: *In vitro* cell viability of (a), the composite acrylamide  $\beta$ -cyclodextrin-g-grafted 3-aminopropyltriethoxysilane bentonite (b) curcumin (CUR)-L-composite, and (c) CUR (triplicates for each sample were analyzed and each datum point represents the mean value $\pm$ standard deviation; n=3)

at pH 2.4 (18.5%) and for pH 7.4 (28.6%). APSB is a good DDS and its efficiency can be improved by grafting process.

The pH of tumour cells is lower than the normal cells. The pH of tumor cells ranges from 5.0 to 6.0. In the present study, the maximum release of CUR is occurring at acidic pH of 6.0, so the developed biodegradable composite is better for the controlled release of CUR to the tumor cells.

The *in-vitro* drug release study was analyzed using Peppas kinetic equation (Fig. 8). In Peppas equation the value of  $k$  gives an idea about the interaction of drug onto the DDS. Smaller the value of  $k$ , weaker is the interaction between the drug and the DDS. The value of  $n$  determines the release mechanism. The fitting of Peppas's kinetic model was analyzed on both AMCD-g-APSB and APSB at pH 6. The value of  $n=0.778$  for AMCD-g-APSB showed that the release of drug follows non-Fickian mechanism. The release of drug depends both on the diffusion of drug and the swelling of the composite. The value of  $k$  for AMCD-g-APSB and APSB are 0.0314 and 0.0743, smaller the value of  $k$  indicates the weaker interaction between the drug and the DDS [37].

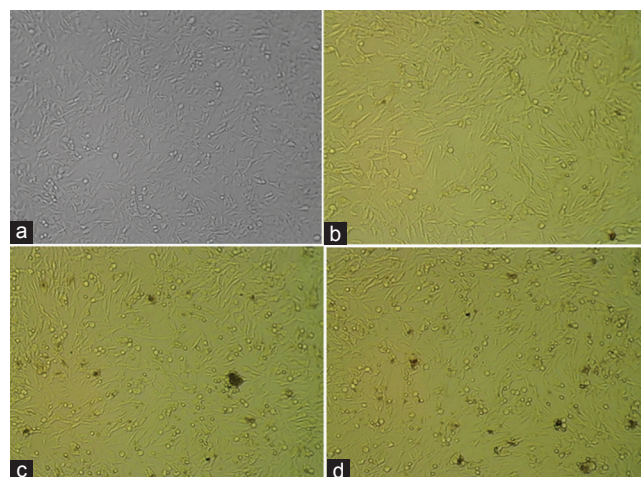


Fig. 10: The images of morphological changes in cells during the cell viability assay. (a) Controlled; (b) acrylamide  $\beta$ -cyclodextrin-g-grafted 3-aminopropyltriethoxysilane bentonite (AMCD-g-APSB) (c) Curcumin (CUR) and (d) CUR-L-AMCD-g-APSB at 5  $\mu$ g/ml images with magnification  $\times 20$  objectives

#### Cell viability analysis

The cell viability was analyzed by MTT method using U87MG cell line incubated to 48 h under variable concentration of 2.5–40.0  $\mu$ g/ml as shown in Figs. 9 and 10. The cell viability of above 80% was considered as cytocompatible and nontoxic [38]. The percentage cell viability of the DDS (AMCD-g-APSB) was not below 80% even at higher concentration of 40.0  $\mu$ g/ml. The percentage cell viability decreases with increase in the concentration of DDS. In the case of the drug-loaded composite, the percentage of cell viability was decreased from 74% to 50.6% when the concentration of drug was increased from 5  $\mu$ g/ml to 10  $\mu$ g/ml. This showed that the percentage of the cell toxicity was increased by the factor 22.4%, when the concentration was doubled [39].

#### CONCLUSION

In the present work, we synthesized a novel drug delivery system by a green synthetic approach. The composite was characterized by FTIR,

XRD, SEM, and differential scanning calorimetry. The swelling behavior of the composite was depending on the pH, time, and composition of the components. The encapsulation efficiency was pH dependent. For a comparative study, the *in vitro* release study of APSB, one of the monomer units of this composite was also carried out. The maximum release of CUR was occurring at a pH 6. The CUR release from AMCD-g-APSB followed non-Fickian mechanism. The release of drug depends on both the diffusion and the swelling of the composite. The *in vitro* MTT assay on U87MG cell line confirmed the biocompatibility of the drug delivery system. The DDS was more potent for the controlled release of CUR to the tumor cells.

#### ACKNOWLEDGMENTS

The authors are expressing sincere gratitude to The Head, Department of Chemistry, Fatima Mata National College, Kollam, for providing laboratory facilities. The corresponding author thanks UGC, New Delhi, for financial assistance in the form of Minor Research Project (2324-MRP/15-16/KLKE015/UGC-SWRO). The authors sincerely acknowledging the services rendered by Indian Institute of Science, Bengaluru, for their assistance in the characterization of the samples.

#### AUTHORS' CONTRIBUTIONS

The work presented here was carried out with the collaboration between all authors.

#### CONFLICT OF INTEREST

There is no conflict of interest.

#### REFERENCES

- Dhivya R, Ranjani J, Rajendhran J, Rajasekaran M, Annaraj J. pH responsive curcumin/ZnO nanocomposite for drug delivery. *Adv Mater Lett* 2015;6:505-12.
- Shome S, Talukdar AD, Choudhury MD, Bhattacharya MK, Upadhyaya H. Curcumin as potential therapeutic natural product: A nanobiotechnological perspective. *J Pharm Pharmacol* 2016;68:1481-500.
- Shanmugam MK, Rane G, Kanchi MM, Arfuso F, Chinnathambi A, Zayed ME, et al. The multifaceted role of curcumin in cancer prevention and treatment. *Molecules* 2015;20:2728-69.
- Bandyopadhyay D. Farmer to pharmacist: Curcumin as an anti-invasive and antimetastatic agent for the treatment of cancer. *Front Chem* 2014;2:1-11.
- Kim S, Stébé MJ, Blin JL, Pasc A. pH-controlled delivery of curcumin from a compartmentalized solid lipid nanoparticle@mesostructured silica matrix. *J Mater Chem B* 2014;2:7910-17.
- Bharti C, Gulati N, Nagaich U, Pal A. Mesoporous silica nanoparticles in target drug delivery system: A review. *Int J Pharm Investig* 2015;5:124-33.
- Carino IS, Pasqua L, Testa F, Aiello R, Puoci F, Iemma F, Picci N. Silica-based mesoporous materials as drug delivery system for methotrexate release. *Drug Deliv* 2007;14:491-5.
- Li Y, Li N, Pan W, Yu Z, Yang L, Tang B. Hollow mesoporous silica nanoparticles with tunable structures for controlled drug delivery. *ACS Appl Mater Interfaces* 2017;9:2123-9.
- Bouchoucha M, Côté M, Rene C, Fortin M, Kleitz F. Size-controlled functionalized mesoporous silica nanoparticles for tunable drug release and enhanced anti-tumoral activity size-controlled functionalized mesoporous silica nanoparticles for tunable drug release and enhanced anti-tumoral activity. *ACS Chemmater* 2016;28:4243-58.
- Thomas J, Kala D, Geroge A. Aminofunctionalised mesoporous silica nanoparticles loaded with 5-Fluorouracil. *Inter J Curr Adv Res* 2017;6:2394-98.
- Wei S, Hongping HE, Jianxi ZH, Peng Y, Yuehong MA, Xiaoliang L. Preparation and characterization of 3-aminopropyl-triethoxysilane grafted montmorillonite and acid-activated montmorillonite. *Chinese* 2009;54:265-71.
- Sørensen MH, Samoshina Y, Claesson PM, Alberius P. Sustained release of ibuprofen from polyelectrolyte encapsulated mesoporous carriers. *J Dispers Sci Technol* 2009;30:892-902.
- Khlibsuwan R, Siepmann F, Siepmann J, Pongjanyaku T. Chitosan-clay nanocomposite microparticles for controlled drug delivery: Effects of the MAS content and TPP crosslinking. *J Drug Deliv Sci Technol* 2017;40:1-10.
- Mandal S, Patil VS, Mayadevi S. Alginate and hydrotalcite-like anionic clay composite systems: Synthesis, characterization and application studies. *Microporous Mesoporous Mater* 2012;30:892-902.
- Sehgal P, Sharma M, Larsen KL, Wimmer R, Daniel E, Doe H. Influence of  $\beta$  cyclodextrin on the mixed micellization process of sodium dodecyl sulfate and sodium lauroyl sarcosine and formation of inclusion complexes. *J Dispers Sci Technol* 2008;29:128-33.
- Ravichandran S, Karthikeyan E. Microwave synthesis-a potential tool for green chemistry. *Inter J Chem Tech Res* 2011;3:466-70.
- Anirudhan TS, Gopal SS, Sandeep S. Synthesis and characterization of montmorillonite/N-(carboxyacyl) chitosan coated magnetic particle nanocomposites for controlled delivery of paracetamol. *Appl Clay Sci* 2014;88:151-8.
- Reddy BH, Rauta RP, Venkatalakshmi V, Sreenivasa S. Synthesis and characterization of novel SA-PA-LSA/C-30B/AG nanocomposite for swelling, antibacterial, drug delivery, and anticancer application. *Asian J Pharm Clin Res* 2018;11:329-30.
- Jain S, Datta M. Montmorillonite-alginate microspheres as a delivery vehicle for oral extended release of venlafaxine hydrochloride. *J Drug Deliv Sci Technol* 2016;33:149-56.
- Ainurofiq A, Nurcahyo I, Yulianto R. Preparation, characterization and formulation of nanocomposite matrix Na-montmorillonite intercalated medium molecular weight chitosan for theophylline sustained release tablet. *Int J Pharm Pharm Sci* 2014;6:131-7.
- Bertuoli PT, Piazza D, Scienza LC, Zattera AJ. Preparation and characterization of montmorillonite modified with 3-aminopropyltriethoxysilane. *Appl Clay Sci* 2014;87:46-51.
- Soppimath KS, Aminabhavi TM. Water transport and drug release study from cross-linked polyacrylamide grafted guar gum hydrogel microspheres for the controlled release application. *Eur J Pharm Biopharm* 2002;53:87-98.
- Kaity S, Isaac J, Kumar PM, Bose A, Wong TW, Ghosh A. Microwave assisted synthesis of acrylamide grafted locust bean gum and its application in drug delivery. *Carbohydr Polym* 2013;98:1083-94.
- Vijan V, Kaity S, Biswas S, Isaac J, Ghosh A. Microwave assisted synthesis and characterization of acrylamide grafted gellan, application in drug delivery. *Carbohydr Polym* 2012;90:496-506.
- Gunathilake TM, Ching YC, Chuah CH. Enhancement of curcumin bioavailability using nanocellulose reinforced chitosan hydrogel. *Polymers* 2017;9:1-19.
- Liu Y, Li Y, Li XM, He T. Kinetics of (3-aminopropyl)triethoxysilane (aPTES) silanization of superparamagnetic iron oxide nanoparticles. *Langmuir* 2013;29:15275-82.
- Su L, Tao Q, He H, Zhu J, Yuan P. Locking effect: A novel insight in the silylation of montmorillonite surfaces. *Mater Chem Phys* 2012;136:292-5.
- Palanikumar L, Choi ES, Cheon JY, Joo SH, Ryu JH. Noncovalent polymer-gatekeeper in mesoporous silica nanoparticles as a targeted drug delivery platform. *Adv Funct Mater* 2015;25:957-65.
- Hu C, Yu L, Zheng Z, Wang J, Liu Y, Jiang Y, et al. Tannin as a gatekeeper of pH-responsive mesoporous silica nanoparticles for drug delivery. *RSC Adv* 2015;5:85436-41.
- Sun R, Wang W, Wen Y, Zhang X. Recent advance on mesoporous silica nanoparticles-based controlled release system: Intelligent switches open up new horizon. *Nanomaterials* 2015;5:2019-53.
- Anirudhan TS, Sandeep S. Synthesis and characterization of a novel pH-controllable composite hydrogel for anticancer drug delivery. *New J Chem* 2011;35:2869-76.
- Pourjavadi A, Hosseinzadeh H, Mazidi R. Synthesis and swelling behaviour of crosslinked kC-g-AMPS superabsorbent hydrogel with antisalt and pH responsiveness properties. *J Appl Poly Sci* 2005;98:255-63.
- Shela TP, Mandowara VK, Gupta DG, Patel SV. Formulation of curcuminoid loaded solid lipid nanoparticles in order to improve oral bioavailability. *Int J Pharm Pharm Sci* 2015;7:278-82.
- Wang YJ, Pan MH, Cheng AL, Lin LI, Ho YS, Hsieh CY, et al. Stability of curcumin in buffer solutions and characterization of its degradation products. *J Pharm Biomed Anal* 1997;15:1867-76.
- Khurana A, Ho CT. High-performance liquid chromatographic analysis of curcuminoids and their photo-oxidative decomposition compounds in *Curcuma longa* L. *J Liq Chromatogr* 1998;11:2295-304.
- Feng F, Nie W, He C, Zhou X, Chen L, Qiu K, et al. Effect of pH-

- responsive alginate/chitosan multilayers coating on delivery efficiency, cellular uptake and biodistribution of mesoporous silica nanoparticles based nanocarriers. *Appl Mater Interfaces* 2014;5:8447-60.
37. Anirudhan TS, Binusreejayan, Jayan PP. Development of functionalized chitosan-coated carboxylated mesoporous silica: A dual drug carrier. *Des Monomers Polym* 2016;19:381-93.
38. Anirudhan TS, Nair SS, Sekhar V. Deposition of gold-cellulose hybrid nanofiller on a polyelectrolyte membrane constructed using guar gum and poly(vinyl alcohol) for transdermal drug delivery. *J Memb Sci* 2017;539:344-57.
39. Liu Y, Pan J, Feng SS. Nanoparticles of lipid monolayer shell and biodegradable polymer core for controlled release of paclitaxel: Effects of surfactants on particles size, characteristics and *in vitro* performance. *Int J Pharm* 2010;395:243-50.